AGU PUBLICATIONS

JGR

Journal of Geophysical Research: Space Physics

RESEARCH ARTICLE

10.1002/2014JA020500

Key Points:
- Field-aligned currents are strongly driven by substorms
- Current magnitude and colatitude rise to a peak after onset and then fall
- More open flux at substorm onset leads to more intense substorms

Correspondence to:
J. C. Coxon,
jcc19@leicester.ac.uk

Citation:
Coxon, J. C., S. E. Milan, L. B. N. Clausen, B. J. Anderson, and H. Korth (2014), A superposed epoch analysis of the regions 1 and 2 Birkeland currents observed by AMPERE during substorms, *J. Geophys. Res. Space Physics*, *119*, 9834–9846, doi:10.1002/2014JA020500.

Received 12 AUG 2014
Accepted 10 NOV 2014
Accepted article online 17 NOV 2014
Published online 15 DEC 2014

A superposed epoch analysis of the regions 1 and 2 Birkeland currents observed by AMPERE during substorms

J. C. Coxon[1], S. E. Milan[1], L. B. N. Clausen[2], B. J. Anderson[3], and H. Korth[3]

[1]Department of Physics and Astronomy, University of Leicester, Leicester, UK, [2]Department of Physics, University of Oslo, Oslo, Norway, [3]Johns Hopkins University Applied Physics Laboratory, Laurel, Maryland, USA

Abstract We perform a superposed epoch analysis of the evolution of the Birkeland currents (field-aligned currents) observed by the Active Magnetosphere and Planetary Electrodynamics Response Experiment (AMPERE) during substorms. The study is composed of 2900 substorms provided by the SuperMAG experiment. We find that the current ovals expand and contract over the course of a substorm cycle and that currents increase in magnitude approaching substorm onset and are further enhanced in the expansion phase. Subsequently, we categorize the substorms by their onset latitude, a proxy for the amount of open magnetic flux in the magnetosphere, and find that Birkeland currents are significantly higher throughout the epoch for low-latitude substorms. Our results agree with previous studies which indicate that substorms are more intense and close more open magnetic flux when the amount of open flux is larger at onset. We place these findings in the context of previous work linking dayside and nightside reconnection rate to Birkeland current strengths and locations.

1. Introduction

The Dungey cycle is the circulation of plasma and magnetic field in the Earth's magnetosphere, driven by its coupling with the solar wind [*Dungey*, 1961]. Magnetic reconnection between the interplanetary magnetic field (IMF), frozen into the solar wind, and terrestrial field lines at the magnetopause creates open magnetic flux interconnecting the interplanetary medium to the polar regions. The motion of the solar wind past the planet leads to these open flux tubes moving antisunward from the dayside to the nightside. Subsequently, reconnection in the tail closes this open magnetic flux, and it returns to the dayside to complete the cycle. It is the opening and closing of flux that drives magnetospheric convection and a sympathetic circulation of plasma in the ionosphere.

Dungey [1961] originally pictured a steady state situation, but it has become obvious that the Dungey cycle is much more dynamic than was first thought, leading to the proposal of the expanding/contracting polar cap (ECPC) paradigm [e.g., *Cowley and Lockwood*, 1992; *Lockwood and Cowley*, 1992]. As dayside reconnection occurs, the amount of open magnetic flux inside Earth's magnetosphere increases. Nightside reconnection reduces the amount of open magnetic flux in the same way. The amount of open magnetic flux in the magnetosphere governs the location of the boundary between the open and closed flux in the ionosphere, enclosing the area known as the polar cap—when there is more open magnetic flux, the boundary is farther from the pole, and therefore, the size of the polar cap is increased [*Milan et al.*, 2007, 2012].

The substorm [*Akasofu and Chapman*, 1961; *Akasofu*, 1964] is an integral component of the ECPC. The substorm cycle comprises three phases: the growth phase, the expansion phase, and the recovery phase [*McPherron*, 1970; *Rostoker et al.*, 1980]. The substorm growth phase, when the auroras move to lower latitudes, is associated with dayside reconnection [*Siscoe and Huang*, 1985]. The expansion phase, when the nightside auroras brighten and move poleward, is associated with the onset of nightside reconnection [*Cowley and Lockwood*, 1992; *Milan et al.*, 2007]. The recovery phase is marked by a dimming of the auroras and a general contraction to higher latitudes as the system returns to quiescent conditions.

It has been noted in previous papers [*Akasofu*, 1975, 2013; *Kamide et al.*, 1999; *Milan et al.*, 2009a] that the intensity of a substorm is associated with the extent of the polar cap at substorm onset; that is to say, the

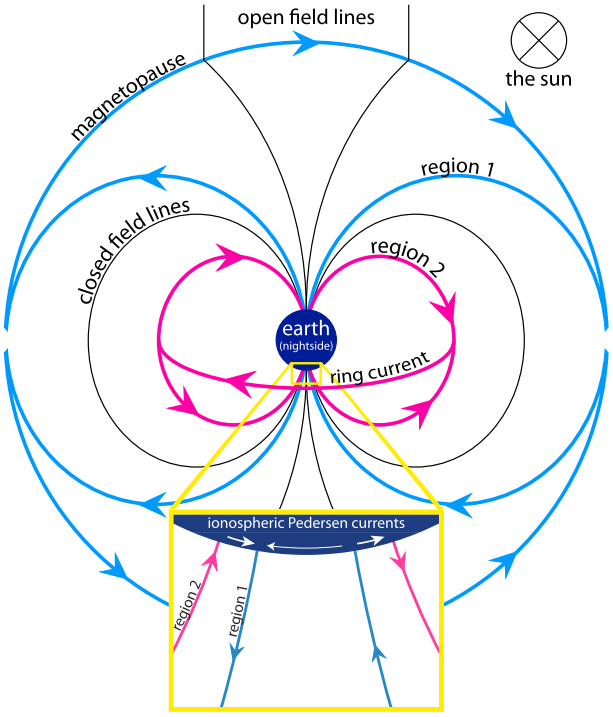

Figure 1. The near-Earth electric current systems drawn as if Earth was eclipsing the Sun. Shown are the region 1, region 2, Pedersen, magnetopause (Chapman-Ferraro), and ring currents as well as the location of open and closed terrestrial magnetic field lines. In the magnification of the southern auroral zone, the arrow showing Pedersen current flow across the polar cap is smaller than the arrows for the auroral zone to indicate the relative strength of the Pedersen currents (not to scale). It can be seen from this image how the region 1 current sheet corresponds to the open/closed field line boundary or OCB.

substorm is stronger when there is more open magnetic flux contained within the polar cap. This occurs because there is more energy stored within the magnetotail, and when a substorm occurs, there is therefore more energy available to dissipate.

Current systems are a ubiquitous component of the magnetosphere, as they transmit stresses around the system. We are particularly interested in the field-aligned currents first proposed at the start of the twentieth century [*Birkeland*, 1908, 1913]. The Birkeland current system is responsible for electrodynamically linking the magnetopause, the inner magnetosphere, and the ionosphere. The large-scale morphology of the currents was first deduced using TRIAD satellite observations [*Iijima and Potemra*, 1976a, 1976b, 1978]. The current system forms two concentric rings above the auroral ionosphere: the poleward (region 1) ring and the equatorward (region 2) ring. *Iijima and Potemra* [1978] observed that the two regions appear to be driven by different parts of the system: the region 1 (R1) currents connect the ionosphere to currents in the magnetopause (also known as the Chapman-Ferraro currents) and the magnetotail and the region 2 (R2) currents connect to the partial ring current in the inner magnetosphere [e.g., *Cowley*, 2000]. The region 1 Birkeland currents are believed to flow, in part, within the boundary between the open and closed flux, also called the OCB [*Clausen et al.*, 2013a]. Region 1 currents flow upward in the dusk sector and downward in the dawn sector, and region 2 currents are of opposite polarity. The regions 1 and 2 currents close through the ionosphere via horizontal Pedersen currents. The system is sketched schematically in Figure 1.

The substorm current wedge (SCW) is a current system linked to the occurrence of a substorm [*Clauer and McPherron*, 1974; *Forsyth et al.*, 2014; *Sergeev et al.*, 2014]. It is linked to the magnetic bay observed in *AL* at the time of substorm onset, which has been noted previously [e.g., *Iijima and Nagata*, 1972; *Gjerloev et al.*, 2004]. Currents are diverted from the magnetotail into the ionosphere, and these currents flow along the field lines, which lead to enhancements in the field-aligned currents during a substorm [*Clausen et al.*, 2013a, 2013b; *Murphy et al.*, 2013].

Clausen et al. [2012] demonstrated that the R1/R2 system moves to higher and lower latitudes in a manner consistent with the ECPC and substorm cycle. *Coxon et al.* [2014] subsequently investigated the magnitude of the current systems, showing that they were consistent with driving by dayside and nightside reconnection. *Clausen et al.* [2013a, 2013b] used a list of 772 substorms detected by the Thermal Emission Imaging System (THEMIS) mission between January and April 2010 to investigate the open flux content during substorms using the location of R1 currents as a proxy. However, they focused on investigating current density over the epoch rather than investigating the current magnitudes. In the present study, we use 2981 substorms detected by SuperMAG over a 3 year period to investigate the dynamics of the current systems during substorms, including both R1 and R2 current magnitudes, and focus on the influence of the open flux content of the magnetosphere at the time of substorm onset.

2. Sources of Data Utilized

2.1. AMPERE and Derived Products

The Active Magnetosphere and Planetary Electrodynamics Experiment (AMPERE) was conceived to investigate the Birkeland currents using magnetometer data from the Iridium®telecommunications satellite network [*Anderson et al.*, 2000]. The Iridium®network of satellites comprises 66 active spacecraft that orbit the Earth in six polar orbital planes at an altitude of 780 km. Eleven spacecraft are found in each plane, and each is in a circular, polar orbit that takes 104 min to complete. These six orbital planes provide measurements along 12 meridians of magnetic local time (two values of magnetic local time (MLT) per orbital plane). *Anderson et al.* [2000] used the cross-track component of the magnetic perturbation measured by the spacecraft to deduce the current density and concluded that the Iridium®constellation data were useful for characterization of large-scale field-aligned currents (FACs) in both hemispheres on time scales of several hours or less. (Strictly speaking, the current density measured by AMPERE is the radial current density; however, in the polar regions, it is very close to the field-aligned current density.)

The AMPERE data set used in the present study contains maps of Birkeland currents in the Northern and Southern Hemispheres, made at 10 min cadence for the period January 2010 to December 2012. In this study we are interested in the large-scale morphology of the R1/R2 system and wish to suppress small-scale, rapidly varying features. To characterize the location and strength of the Birkeland current ovals, we use a fitting method developed by *Clausen et al.* [2012] and *Coxon et al.* [2014].

We fit a sinusoid multiplied by a Gaussian to the current density along each MLT to identify the two signatures associated with R1 and R2. Taking each value of MLT for which a successful fit was achieved, the R1 and R2 signatures are integrated over both latitude and longitude. We then take the dawn sector MLTs, sum the results of the integration, and multiply by $12/n$ where n is the number of successful fits achieved in the dawn sector. The process is repeated for dusk, such that we obtain the total R1 and R2 current flow in the dawn and dusk sectors. The absolute values of the two R1 currents and the absolute values of the two R2 currents are then summed to find J_1 and J_2, respectively, which are the total current flowing measured in amperes [*Coxon et al.*, 2014].

The latitudes of the peak current density associated with R1 and with R2 can be found in the fit we achieve [*Clausen et al.*, 2012]. We fit an oval to these latitudes to find the location of the Birkeland current ovals, described by l_1 or l_2 plus a cosine term (for the R1 or R2 current oval, respectively). Where there are no successful fits at the time of substorm onset, we eliminate the substorm from consideration, leaving 2900 substorms. It should be noted that the l_1 and l_2 parameters are properly described as the number of degrees of latitude from the geomagnetic pole; while this is equivalent to colatitude in the Northern Hemisphere, in the Southern Hemisphere it is the colatitude subtracted from 180°. However, for ease of description, we will use the term "colatitude" to refer to these parameters in both hemispheres.

2.2. OMNI and Derived Products

The OMNI data set provides time series of solar wind parameters propagated to their impact on the bow shock [e.g., *King*, 1991; *Papitashvili et al.*, 2000, and references therein]. We use data from OMNI to estimate the dayside reconnection rate Φ_D, using the expression by *Milan et al.* [2012]:

$$\Phi_D = L_{\text{eff}}(V_X) V_X B_{YZ} \sin^{\frac{9}{2}}\left(\frac{\theta}{2}\right) \tag{1}$$

In the above equation $L_{\text{eff}}(V_X)$ is an effective length scale, given by

$$L_{\text{eff}}(V_X) = 3.8 R_E \left(\frac{V_X}{4\times 10^5 \text{ms}^{-1}}\right)^{\frac{1}{3}} \tag{2}$$

and B_{YZ} is the transverse component of the IMF, given by

$$B_{YZ}^2 = B_Y^2 + B_Z^2. \tag{3}$$

V_X is the solar wind speed, θ is the clock angle between the IMF vector projected into the GSM Y-Z plane, and Z axis and R_E is the radius of Earth. The dayside reconnection rate is the rate at which flux is transferred by the reconnection electric field across the effective length L_{eff} and is therefore given by equation (1) in volts.

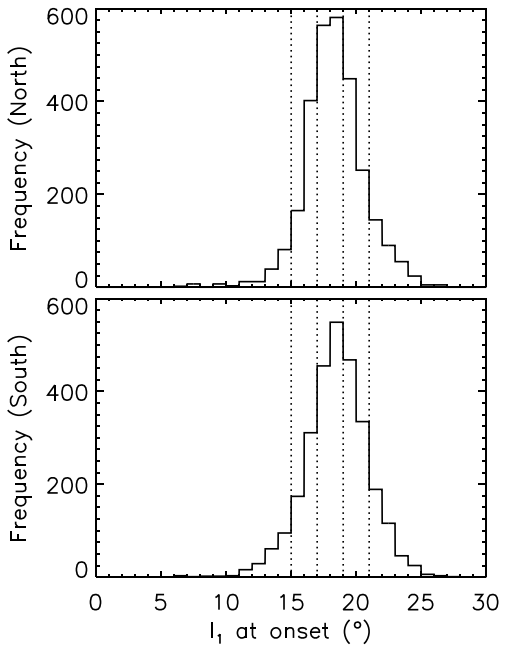

Figure 2. Histograms showing the value of l_1 for the region 1 current oval at $t = 0$ min (substorm onset) for the (top) Northern and (bottom) Southern Hemispheres. Larger values of l_1 at onset imply more active geomagnetic conditions prior to the onset of the substorm. The dotted lines show the boundaries of bins defined in section 2.3.

2.3. SuperMAG

The SuperMAG data set collates and unifies magnetometer data from across the globe [*Gjerloev*, 2009, 2012]. SMU and SML are SuperMAG-calculated equivalents of the electrojet indices *AU* and *AL*. An automated procedure identifies substorm onsets in these indices [*Newell and Gjerloev*, 2011a, 2011b]. We have used the SuperMAG substorm onset list for the period 2010 to 2012, coincident with the AMPERE data used in the present study, which contains approximately 3000 substorms. We filter out those substorms for which the onset MLT reported by SuperMAG is on the dayside, i.e., where $6 \leq \mathrm{MLT} \leq 18$. We use the colatitude of the R1 current oval recorded by AMPERE, l_1, at the time of each substorm as a proxy for the open magnetic flux content of the magnetosphere prior to onset [see also *Milan et al.*, 2009b].

The distribution of the onset colatitudes of the SuperMAG substorm list is presented in Figure 2, which shows substorms distributed between ~10° and ~25° and a peak measured at an onset colatitude of 18°. The number of substorms in each bin varies somewhat between the Northern and Southern Hemispheres, with ~550 substorms seen at the peak in the Northern Hemisphere and ~500 substorms in the Southern Hemisphere. However, the distribution in both hemispheres is similar.

As such, five bins are defined into which substorms can be sorted by onset colatitude. We denote these bins as I–V and define them as follows. I: $0° < \phi \leq 15°$; II: $15° < \phi \leq 17°$; III: $17° < \phi \leq 19°$; IV: $19° < \phi \leq 21°$; and V: $21° < \phi \leq 30°$. We return to this categorization in section 4.2.

3. Observations of the Birkeland Currents Made by AMPERE

Figure 3 shows the interval between midnight on 28 June 2010 and midnight on 3 July 2010. Figures 3a and 3b show cuts through the dawn-dusk meridian of the current density observed by AMPERE. Figure 3a shows the Northern Hemisphere, whereas Figure 3b shows the Southern Hemisphere. Figures 3a and 3b show the densities of the currents as well as their extent in latitude, but in order to examine the current magnitudes, we turn to Figure 3c, which depicts the current magnitudes J_1 and J_2 for the Northern Hemisphere measured using our technique for analyzing the AMPERE data set [*Coxon et al.*, 2014]. Figure 3d shows the ratio J_1/J_2: when the ratio is above 1, the R1 current flowing is stronger than the R2 current. Figure 3e shows the dayside reconnection rate Φ_D determined using equation (1). Figure 3f shows the *AL*/*AU* indices, and the dotted lines indicate substorm onsets given by SuperMAG for this time period [*Newell and Gjerloev*, 2011a, 2011b].

The plot depicted in Figure 3 is of an active period. In Figure 3e, Φ_D reaches values of 40 kV on several occasions and exceeds 100 kV near midnight on 30 June. Two periods of very high dayside reconnection rate are associated with two coincident enhancements in the current magnitudes, consistent with the relationship between reconnection and current magnitude found by *Coxon et al.* [2014]. The opening of magnetic flux that occurs during dayside reconnection also leads to equatorward expansions of the currents observed in Figures 3a and 3b, consistent with the ECPC paradigm [*Cowley and Lockwood*, 1992] as discussed by *Clausen et al.* [2012].

Also seen are magnetic bays in the SML index in Figure 3f, which are associated with substorm onset. Twenty-four substorms are identified in the period indicated, and the current magnitudes are enhanced as a result of substorm onset in most of the substorms depicted in Figure 3. The ratio J_1/J_2 is also enhanced

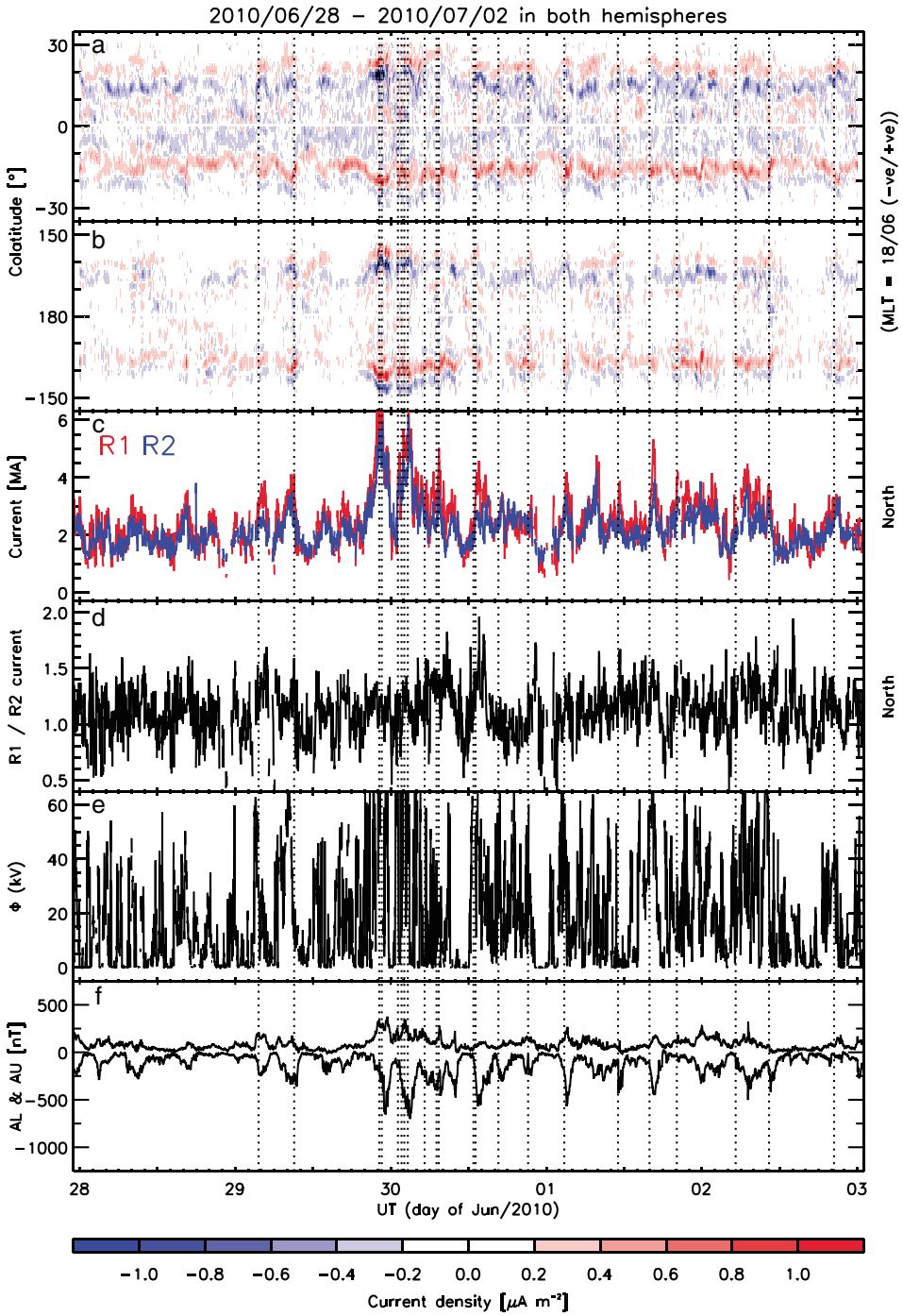

Figure 3. Substorm-related parameters for a period beginning at midnight on 28 June 2010 and ending at midnight on 3 July 2010. From top to bottom, keograms showing the dawn-dusk meridian for (a) the Northern Hemisphere and (b) the Southern Hemisphere; (c) the R1 current magnitude J_1 and R2 current magnitude J_2 for the Northern Hemisphere; (d) J_1/J_2 in the Northern Hemisphere; (e) the dayside reconnection rate Φ_D; and (f) the *AL* and *AU* indices. Vertical dashed lines represent the locations of substorms as given by SuperMAG. The reader should be aware that upward and downward currents are denoted by red and blue in Figures 3a and 3b (as given by the key at the bottom of the figure), but red and blue are used to denote R1 and R2, respectively, in Figure 3c.

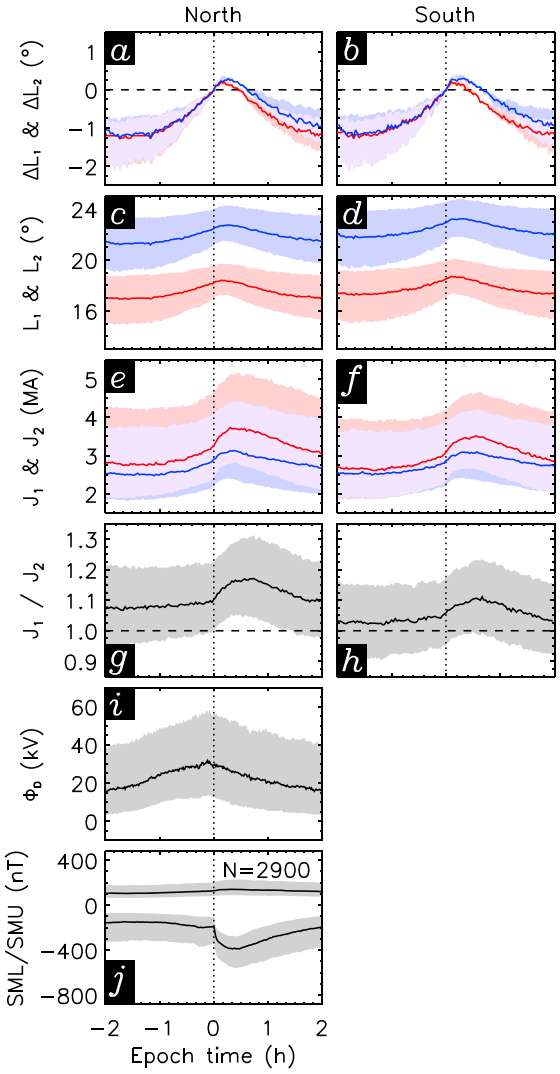

Figure 4. (a and b) Δl_1 and Δl_2 in degrees, (c and d) l_1 and l_2 in degrees, (e and f) J_1 and J_2 (MA), (g and h) J_1/J_2, (i) Φ_D (kV), and (j) SML and SMU (nT) plotted against the epoch time t in minutes on the x axis for the Northern Hemisphere (left) and Southern Hemisphere (right). R1 and R2 are denoted by red and blue, respectively. It should be noted that the scales in this figure are different from those used in subsequent figures.

after substorm onset in a number of cases. Looking at Figures 3a and 3b, the current ovals appear to expand at substorm onset and contract in response to the onset of nightside reconnection in a substorm [*Clausen et al.*, 2012]. In order to examine these phenomena more quantitatively, we perform a superposed epoch analysis to see the general trends over 3 years of AMPERE data.

4. Superposed Epoch Analysis

We use the substorm onset times identified by SuperMAG to form a superposed epoch analysis of the parameters of interest, including the R1 and R2 current magnitudes J_1 and J_2, oval colatitudes l_1 and l_2, dayside reconnection rate Φ_D, and geomagnetic indices SMU and SML. The analysis covered the period from 2 h before substorm onset to 2 h after. In the first instance we performed the analysis on all 2900 substorms. Subsequently, we performed the analysis on subsets of substorms binned by onset colatitude. There are cases in which substorm onsets occur within 2 h of one another (so that the 4 h window would contain multiple substorms; a case which can clearly be seen around midnight on 30 June 2010 in Figure 3); we did not filter out any onsets based on this criterion, however, such that the analysis presented includes some cases of substorm onsets occurring within 2 h of one another.

In Figures 4–7, solid lines are used to indicate the median of the data plotted, while shaded areas are drawn which describe the upper and lower quartiles of the data in each plot. In order to differentiate between R1 and R2 currents, we use red and blue respectively for both the solid lines and shaded areas. Purple shading is used to indicate the areas in which the quartiles overlap.

4.1. Quantifying the Reaction of the Coupled Magnetosphere-Ionosphere System to Substorms

In Figure 4 the median response of the Birkeland currents to substorm onset is shown. From top to bottom: the variation of colatitude l_1 relative to the onset colatitude, the variation in l_1, the variation in the R1 and R2 current magnitudes, the ratio R1/R2, the expected dayside reconnection rate Φ_D, and the SML/SMU indices [*Newell and Gjerloev*, 2011a]. For ease of reading, we describe SML in terms of its magnitude, neglecting the sign of the perturbations it measures, which means that an increase in SML would indicate a transition to more negative magnetic perturbations.

In Figures 4a–4d, we see the change in position of the current ovals as measured by l_1. We see the current ovals expand to lower latitudes (higher colatitudes) as substorm onset approaches and then begin to contract again at $t \sim 10$ min. The R1 current oval starts at approximately 17°, whereas R2 starts at approximately 21°—both ovals expand and then contract back to their preonset state. The change in the latitudinal extent of the current ovals varies over a range of 2° latitude during the 4 h period, as demonstrated by Figure 4a, in which Δl_1 is seen to vary between −1.5 and 0.5 (with the latter value occurring 10 min subsequent

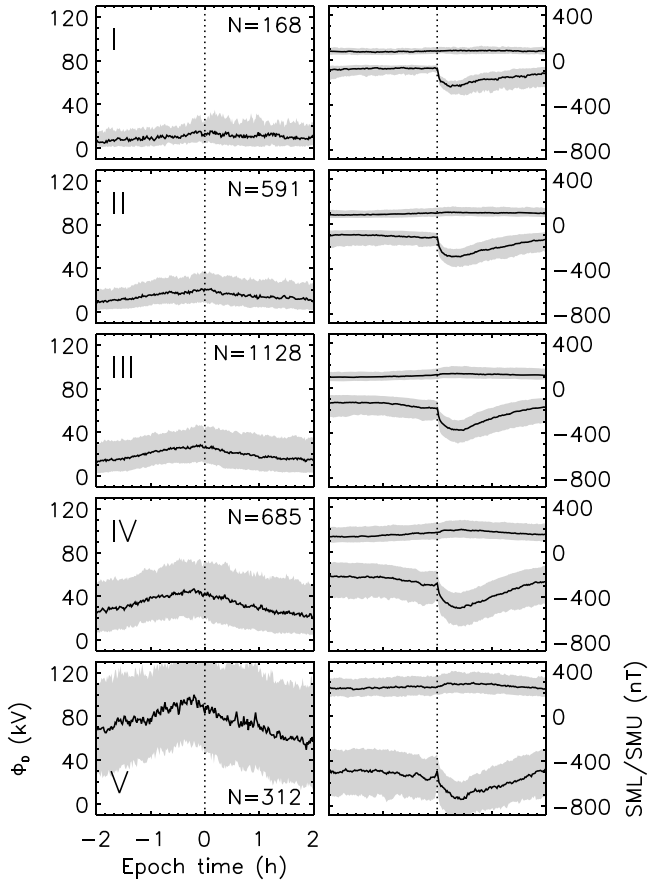

Figure 5. (left column) Φ_D as calculated using OMNI data and (right column) SML/SMU with respect to substorm onset at $t = 0$ min, binned by substorm onset colatitude (increasing from top to bottom). N is the number of substorms in the relevant bin.

to onset). Both current ovals are seen to expand at the same rate until onset, at which point R2 starts to expand faster, indicating a broadening in latitude of the current system. It also indicates that R2 is more sluggish than R1 in its return to pre-substorm levels.

The current magnitudes as measured by AMPERE start, in the Northern Hemisphere, at $J \sim 2.75$ MA in Figure 4e and a ratio R1/R2 of ~1.075 in Figure 4g. The current magnitudes slowly increase between $t = -120$ min and $t = 0$ min, before substorm onset leads to a more rapid increase and a peak in current magnitude of $J \sim 3.75$ MA at $t \sim 20$ min. The current magnitudes observed then decrease through the period, returning almost to their initial levels. The ratio follows an almost identical pattern, with a slow increase observed until substorm onset, a rapid increase to a peak value of approximately 1.2 at $20 < t < 40$ min and then returning to preonset levels. The Southern Hemisphere follows a similar behavior, but the current magnitude (Figure 4f) and ratio (Figure 4h) are lower throughout the epoch.

In Figure 4i, the dayside reconnection rate $\Phi_D \sim 15$ kV at $t = -120$ min. It increases as time progresses, with a peak of $\Phi_D \sim 30$ kV slightly before substorm onset at $t = 0$ min. The level of dayside reconnection then falls, returning to its initial value at the end of the interval. In Figure 4j, SMU ~100 nT at $t = -120$ min, whereas SMU ~ −150 nT at that point. SMU increases slightly from the start of the period, with a peak occurring at $t \sim 20$ min. The same is seen in SML until $t = 0$ min at which point a pronounced magnetic bay can be seen in SML at the time of substorm onset [*Rostoker et al.*, 1980]. This signature marks the formation of the substorm current wedge and is a recognized signature of substorm onset. Both SML and SMU then begin to decrease in magnitude through the epoch, returning to almost preonset levels at the end of the period.

4.2. The Variation of Reactions to Substorms Given Different Levels of Activity

4.2.1. Reconnection Rate and Magnetic Indices

Turning now to the colatitude of onset categories established in section 2.3, Figure 5 shows the dayside reconnection rate Φ_D alongside SML/SMU averaged for the five categories outlined. These categories are defined by the colatitude of the R1 current oval at substorm onset. The plots corresponding to the smallest onset colatitudes (and thus the lowest level of activity) are depicted at the top of the figure and the plots for the largest onset colatitudes depicted at the bottom.

In Bin I, it can be seen that at $t = -120$ min, $\Phi_D < 10$ kV and continues at that rate until $t = -20$ min. At this point, the reconnection rate begins to increase to a peak of approximately 15 kV located subsequent to the substorm onset. In Bin II, the reconnection rate increases from the initial value (~10 kV) to the peak (~20 kV), which is located at substorm onset. In Bins III–V, the initial and peak values increase until in Bin V, Φ_D varies between approximately 70 and 100 kV. The location of the peak in dayside reconnection

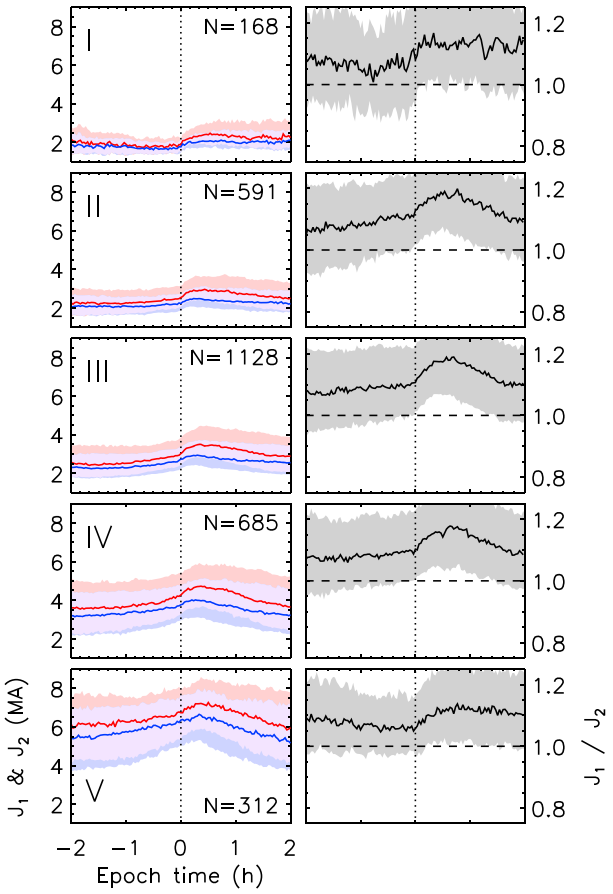

Figure 6. (left column) The magnitude in the Northern Hemisphere of the region 1 (J_1, red) and region 2 (J_2, blue) currents and (right column) the ratio $\frac{J_1}{J_2}$ with respect to substorm onset at $t = 0$ min, binned by substorm onset colatitude (increasing from top to bottom). *N* is the number of substorms in the relevant bin.

rate gets earlier with bin: in Bin I, the peak is seen just after substorm onset, whereas the peak in Bin V is as much as 25 min prior. The peak value is approximately double the initial value in Bin I, whereas in Bin V the peak value is ~140% that of the initial value.

Turning to SML and SMU in Bin I, it is observed that both appear flat between the start of the interval (~90 nT) and the onset of the substorm. At substorm onset, SMU increases by perhaps 10 nT but returns to its initial magnitude relatively quickly. The familiar magnetic bay in SML is present at onset, with the SML magnitude increasing to ~200 nT and remaining higher than the initial magnitude for the rest of the interval. The sudden increase and then gradual decrease to a level higher than the initial magnitude is a common feature in every bin.

In Bin II, both SML and SMU remain steady at their initial values (100 nT and 90 nT, respectively) until the substorm onset, at which point SMU increases slightly before quickly returning to its original level. SML again shows the signature magnetic bay, increasing to a higher magnitude of 300 nT. In Bins III–V, the magnitude of both indices increases slowly from $t = -120$ min to $t = 0$ min. At onset, the rate of increase of SMU climbs before the peak approximately 20 min later—it then returns to pre-substorm levels. The initial/peak magnitudes of SMU and SML increase with the bays: in Bin V, the initial value of SML is approximately 500 nT, increasing to 750 nT just after onset. SMU starts at 250 nT and increases to 300 nT before dropping back down again. In all bins we see a decrease in SML magnitude just prior to onset, although it is most pronounced in Bins IV and V.

4.2.2. Current Magnitudes

Figure 6 shows J_1, J_2 and J_1/J_2. In Bin I, the observed current magnitudes remain uniform at ~2 MA until onset which causes an increase in magnitude to an approximate value of 2.5 MA in R1 and 2.25 MA in R2. The currents appear to stay at this magnitude for the rest of the interval shown. Initially, R1 is higher than R2 at a ratio of 1.05; at onset, the ratio between the two increases to a value of 1.2, and the ratio then decreases to 1.1 over the 2 h subsequent to onset.

In Bin II, the initial values of the currents are just above 2 MA. The current systems remain steady until onset, when relatively rapidly increase; R1 to J ~3 MA and R2 to J ~2.5 MA at $t = 20$ min. They then decrease gradually toward their initial value as time progresses. The ratio starts at a value of 1.05 and increases slightly until onset, at which point it climbs to a value of 1.15 and decreases slowly through the rest of the period.

In Bin III, the initial value of the currents is around 2.5 MA, with an increase at onset to 3.5 MA in R1 and 3 MA in R2. The slow decrease that subsequently occurs leads to values at $t = 120$ min that are between 0.25 and 0.5 MA higher than initially. The ratio starts above 1.05 and increases to 1.2 before decreasing, again to a value slightly higher than the initial value. Bin IV sees an initial R1 and R2 magnitude of just above 3.5 MA

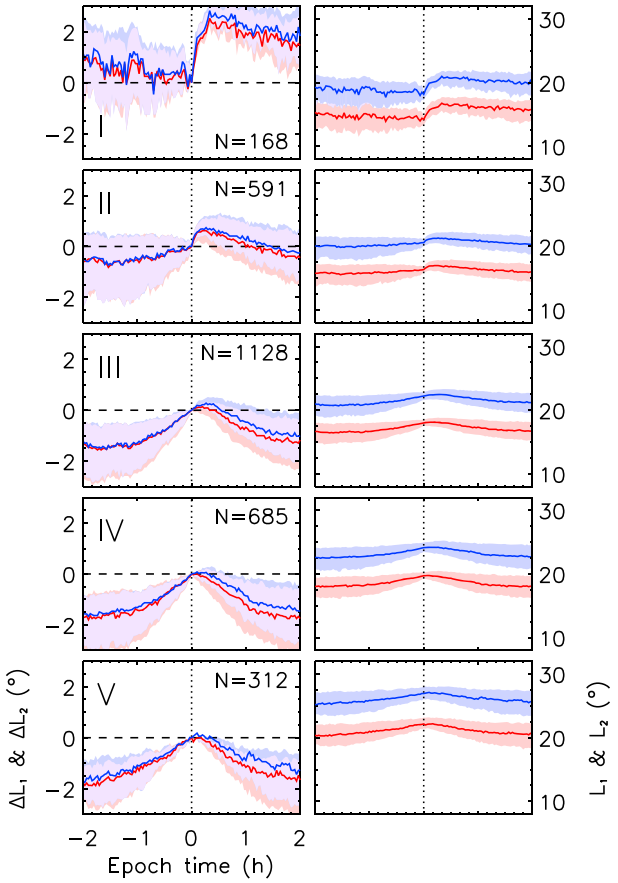

Figure 7. I_1 (red) and I_2 (blue) in the Northern Hemisphere with respect to substorm onset at $t = 0$ min, binned by substorm onset colatitude (increasing from top to bottom). The left-hand plots show the value of I_1 and I_2, whereas the right-hand plots show $I_{1,t} - I_{1,0}$ (and the same for I_2). The units are equivalent to the average colatitude of the current oval. *N* is the number of substorms in the relevant bin.

and 3 MA, respectively, which increase to 4.75 MA and 4 MA at $t = 20$ min before decreasing to values comparable to those at the start. The ratio in this case starts between 1.05 and 1.1 before climbing to 1.2 and then returning. In Bin V, the R1 and R2 magnitudes are 6 and 5.5 MA, respectively, and they increase to a peak magnitude of 7 MA and 6.5 MA, again at $t = 20$ min, before decreasing to values of 6 MA and 5.5 MA. The ratio starts at 1.1, decreases toward onset, and climbs very slightly at onset before returning to its original value.

The peak of the current magnitudes and ratios observed is consistently seen at $t = 20$ min, which does not appear to change with the variation in onset latitude. The increase in current magnitude coincidental with the substorm onset appears to be consistently larger for the region 1 current than for the region 2 current, matching the observed increase in ratio between the two at onset.

4.2.3. Latitude of Current Ovals

Figure 7 shows the value of I_1 and I_2 averaged per bin. In this case, Bin I shows that the current ovals get smaller by 0.5–1° from the beginning of the interval depicted until the onset of the substorm at $t = 0$ min, with a sharp increase seen at the onset of the substorm. The size of the current oval increases by 2° before decreasing throughout the period (at $t = 120$ min, they remain larger than their initial values). The two current ovals change in size similarly through the interval, but with I_1 decreasing in size more quickly than I_2 before the onset of the substorm and then increasing in size more quickly, reaching a higher ΔI.

In Bin II, the two current ovals increase slowly in size by ~1° from the start of the period until substorm onset, both current ovals showing the same increase in size. After onset, both current systems increase more rapidly, until both current ovals reach a peak of ~1° larger at t ~20 min. The R2 current oval increases in size to a higher extent than R1, and ΔI_2 remains larger than ΔI_1 with the current ovals remaining ~0.25° larger at the end of the epoch than at the start.

Bin III exhibits a similar pattern prior to substorm onset, with both current systems increasing in tandem by 1.5° and the decrease in size after the peak being almost identical to Bin II. In this case, however, there is no increase in the rate of oval growth at the point of onset, with the peak in oval size occurring at t ~10 min. In Bin IV, the currents increase by 2° and the peak again moves earlier, to $t = 0$ min, with the ovals at the end of the epoch being approximately 0.25° larger than at the beginning, as in Bins II and III. In Bin V, the peak is also at $t = 0$ min but the ovals are 0.5° larger than their pre-substorm size at the end of the epoch, and the total increase is 2°.

As the onset colatitude increases with bin, the disparity between ΔI_2 and ΔI_1 increases. So too does the difference between I_1 and I_2, with the two current ovals being separated by 8° in Bin I but by 10° in Bin V.

5. Discussion

In the ECPC paradigm, substorm growth and expansion phases manifest themselves as the expansion and contraction of the polar cap [*Cowley and Lockwood*, 1992], and so we discuss the spatial variation in the Birkeland current systems in that context. Ionospheric convection is driven through first dayside and then nightside reconnection and the subsequent motion of flux tubes in the magnetosphere [*Milan*, 2013]. These ionospheric motions are resisted by frictional coupling with the neutral atmosphere, requiring horizontal ionospheric currents and field-aligned currents. Hence, both phases are expected to be associated with FAC enhancements, as demonstrated by *Coxon et al.* [2014], and we explore the relationship in more detail. We also utilize the categories in section 2.3 to discuss how the amount of open flux in the magnetosphere at onset affects the reaction of the Birkeland current system to substorms [*Milan et al.*, 2009a].

5.1. The Reaction of the Birkeland Currents to Substorms

5.1.1. Spatial Variations

As described in section 1, the polar cap expands as the amount of open flux in the magnetosphere increases. The R1 currents flow along the OCB (section 1), and so the motion of the R1 current oval can be used as a proxy for the polar cap boundary, indicating that we should see similar expansions and contractions to those seen in auroral data [*Milan et al.*, 2003; *Clausen et al.*, 2013b]. In Figure 4 the extent of the current ovals expands through the growth phase as open flux is added by dayside reconnection. After substorm onset, the ovals maximize and then begin to contract again, which is consistent with open flux being closed in the magnetotail during the substorm expansion phase. Therefore, the current ovals can be used as a proxy for the amount of open flux in the magnetosphere, and the time derivative of I_1 could be used to examine dayside and nightside reconnection rates.

The amount of open flux maximizes at the same time as the extent of the current ovals, at t ~20 min, just after the onset of the substorm expansion phase. This indicates that although the dayside reconnection rate begins to wane immediately prior to onset, Φ_D is still higher than the nightside reconnection rate Φ_N until the point that the open flux content begins to decrease again. This indicates that Φ_N becomes larger than Φ_D just prior to the maximum of the magnetic bay observed in SML. We therefore infer that it marks the peak of Φ_N.

5.1.2. Magnitude Variations

It can clearly be seen that field-aligned currents are strongly driven by substorms. The currents increase in magnitude as Φ_D increases, with rises in both clearly observed in Figure 4. This indicates that dayside reconnection drives currents through the Birkeland current system during the substorm growth phase. It was previously shown by *Coxon et al.* [2014] that the magnitude of the Birkeland currents gets larger with increases in the value of Φ_D and also the *AL* index, consistent with the result here. The total increase in the current magnitude over the substorm cycle is 1 MA.

At substorm onset, the growth phase of the substorm is over, and the dayside reconnection rate on average begins to drop [*Freeman and Morley*, 2009] but the current magnitudes continue to increase. Since the onset of the substorm implies that magnetic reconnection has initiated in the magnetotail, we can infer that this is due to driving from the nightside reconnection increasing as the dayside reconnection rate decreases and represents part of the expansion phase of the substorm. Our inference is corroborated by an examination of the current densities over a 2 h epoch performed by *Clausen et al.* [2013a]. The fact that the current magnitudes reach their peak coincident with the extent of the current ovals indicates that it is the point at which the sum of reconnection rates $\Phi_D + \Phi_N$, related to the total cross polar cap potential [*Milan*, 2013], is at its peak.

The substorm current wedge also drives current through the Birkeland current system, causing the currents to increase more rapidly; the increase is a signature of the substorm expansion phase that can be seen in SML, which measures the magnetic perturbation associated with the substorm current wedge (SCW). As the SCW begins to decrease in magnitude so too does SML, coinciding with an expected decrease of the Birkeland currents. This is consistent with observations by *Murphy et al.* [2013] which show that both regions 1 and 2 are enhanced during the substorm cycle but is inconsistent with observations that substorms are seen only in the R1 currents [*Clausen et al.*, 2013b].

It is clear that field-aligned currents are strongly driven by magnetic reconnection events in the solar wind-magnetosphere coupled system. The magnitude of the two current systems increases by up to 1 MA

over the course of a substorm cycle, but the two current systems do not react identically to the onset of a substorm. The disparity in reaction can be seen by examination of the ratio J_1/J_2, which increases to as much as 1.2 after substorm onset. The increase implies proportionally more current flowing through R1, even though both current systems are enhanced. This may explain why previous observations of AMPERE data have differed on the role of R2 during the substorm cycle [*Murphy et al.*, 2013; *Clausen et al.*, 2013b]: our observations suggest that although R1 experiences a more notable enhancement, both current systems react to substorms. R1 experiencing larger enhancements than R2 is consistent with previous examinations of substorms [*Sergeev et al.*, 2014].

The high ratio suggests that more R1 current closes across the noon/midnight meridian through the ionosphere during the substorm expansion phase, probably indicating significant current closure through the substorm auroral bulge. Usually, Hall currents flow sunward across the polar cap and antisunward around the flanks of the polar cap (also called the DP-2 current system), with Pedersen currents flowing in the auroral zone and also duskward across the polar cap. In this case, R1 currents can either close through R2 currents (via the auroral zone) or through R1 currents on the opposite side of the polar cap. During the substorm expansion phase, the substorm electrojet (also called DP-1) flows westward across midnight (from the dawn sector to the dusk sector), meaning that more R1 current can flow duskward and close through R1, explaining how the onset of expansion phase can increase the relative strength of R1 to R2.

Finally, the Birkeland currents decrease both in magnitude and in spatial extent after the expansion phase, as the recovery phase leads back into a quiescent magnetospheric state.

5.2. Reactions Varying With Geomagnetic Conditions

Bins I–V show the change in the reaction of the Birkeland currents to substorms as the current ovals at onset are more equatorward (Figures 5–7). Bin I merits a separate discussion, presented in section 5.2.1.

Within Bins II–V, it has been observed that the dayside reconnection rate is higher as the onset colatitude of the current ovals increases, which is also true for SML and SMU (Figure 5). In order for the current oval to reach high colatitudes, the dayside reconnection rate must be high to add enough open flux to expand the oval before the start of nightside reconnection at substorm onset. As such, this is consistent with existing pictures of the ECPC paradigm.

As explained in section 1, substorm onsets that occur with higher amounts of open magnetic flux are more intense due to the higher amount of energy contained within the magnetotail [*Milan et al.*, 2009a]. This explains the larger magnetic bay in SML subsequent to substorm onset, as a more intense substorm is triggered. It also explains why the negative change in I_1 and I_2 is larger as the onset colatitude represented by the bins increases, since open magnetic flux is closed in the magnetotail at a higher rate and thus the polar cap will contract more quickly (Figure 7). It should be remembered, however, that I_1 and I_2 do not vary linearly with the open flux content of the magnetosphere.

The Birkeland current magnitudes become more enhanced at all points of the epoch, per bin, as the onset colatitude increases. Since the current magnitudes are associated with higher reconnection rates, the higher Φ_D values observed with onset colatitude are evidently responsible for driving the increase. As described, the ratio J_1/J_2 at the start of the epoch is larger as the onset colatitudes increase, indicating that R1 currents are relatively larger than R2 currents with higher geomagnetic activity, consistent with previous observations [*Coxon et al.*, 2014]. The enhancement in the ratio that occurs after substorm onset becomes less obvious from Bin II to Bin V, however. We conclude that this indicates that the enhancement to the Birkeland currents is more evenly spread between R1 and R2 as conditions become more extreme or that the SCW intensity does not depend on onset latitude (Figure 6).

5.2.1. Signatures Seen at Small Substorm Onset Colatitudes

Contrary to the other bins, Bin I shows a decrease in SML, SMU, I_1, I_2, J_1, and J_2 prior to onset. At onset, there is a sudden increase in these values. Unlike the other bins, which show Φ_D increasing over the 2 h preceding onset, the dayside reconnection rate begins to increase approximately 20 min prior to onset and remains high until after onset, which would result in the coupled solar wind-magnetosphere system experiencing the addition of open flux during the substorm. This would therefore lead to SMU increasing with enhanced ionospheric convection and an increase in the size of the current ovals, both of which are seen just after the dayside reconnection rate has increased.

Within the context of the ECPC paradigm, a decrease in the extent of the current ovals indicates that the amount of open flux contained within the polar cap decreases between the start of the epoch and the point of substorm onset. Such a decrease can only be explained by magnetic reconnection on the nightside causing the conversion of open to closed flux, which could imply reconnection at a distant neutral line in the magnetotail during extremely quiescent periods.

6. Conclusions

The work described in this paper gives an overview of the reaction of the Birkeland current system (in both magnitude and spatial extent) to substorms within the context of the expanding/contracting polar cap paradigm. We have demonstrated their reaction during various phases of the substorm and show that they become more intense in the growth phase and reach a maximum during the expansion phase soon after onset, decreasing to pre-substorm levels in the recovery phase.

These results can be interpreted in the framework of currents being driven by ionospheric flows which are ultimately driven by magnetic reconnection. The magnitude of the two current systems increases by up to 1.25 MA over the course of a substorm cycle, and the ratio J_1/J_2 increases to as much as 1.2 after substorm onset, suggesting that the SCW enhances both Birkeland current systems but preferentially flows through the poleward region 1 currents.

We categorize the data by colatitude and assume that larger current ovals imply a larger polar cap and therefore more open flux. The change in the size of the current ovals can be used to pinpoint the stage at which nightside reconnection begins to dominate over dayside reconnection, and we show that nightside reconnection occurs at a higher rate after substorm onset when the current ovals (and therefore the amount of open magnetic flux) are higher.

Acknowledgments

J.C.C. was supported by a Science and Technology Funding Council (STFC) studentship. S.E.M. was supported on STFC grant ST/K001000/1. For the Iridium-derived AMPERE data (http://ampere.jhuapl.edu/), we acknowledge the AMPERE Science Center. For the OMNI data (http://omniweb.gsfc.nasa.gov/), we acknowledge use of NASA/GSFC's Space Physics Data Facility's CDAweb service. For the SuperMAG indices and substorm list (http://supermag.jhuapl.edu/), we acknowledge Intermagnet; USGS, Jeffrey J. Love; CARISMA, PI Ian Mann; CANMOS; the S-RAMP Database, PI K. Yumoto and K. Shiokawa; the SPIDR database; AARI, PI Oleg Troshichev; the MACCS program, PI M. Engebretson, Geomagnetism Unit of the Geological Survey of Canada; GIMA; MEASURE, UCLA IGPP and Florida Institute of Technology; SAMBA, PI Eftyhia Zesta; 210 Chain, PI K. Yumoto; SAMNET, PI Farideh Honary; the institutes who maintain the IMAGE magnetometer array, PI Eija Tanskanen; PENGUIN; AUTUMN, PI Martin Connors; DTU Space, PI Jürgen Matzka; South Pole and McMurdo Magnetometer, PI's Louis J. Lanzarotti and Alan T. Weatherwax; ICESTAR; RAPIDMAG; PENGUIn; British Artarctic Survey; McMac, PI Peter Chi; BGS, PI Susan Macmillan; Pushkov Institute of Terrestrial Magnetism, Ionosphere and Radio Wave Propagation (IZMIRAN); GFZ, PI Monika Korte; SuperMAG, and PI Jesper W. Gjerloev. We also acknowledge the International Space Science Institute, Bern, Switzerland, for hosting discussions which informed the study. We would like to thank the reviewers for their comments.

Larry Kepko thanks Martin Connors and W. Jeffrey Hughes for their assistance in evaluating the paper.

References

Akasofu, S.-I. (1964), The development of the auroral substorm, *Planet. Space Sci.*, *12*(4), 273–282, doi:10.1016/0032-0633(64)90151-5.

Akasofu, S.-I. (1975), The roles of the north-south component of the interplanetary magnetic field on large-scale auroral dynamics observed by the DMSP satellite, *Planet. Space Sci.*, *23*(10), 1349–1354, doi:10.1016/0032-0633(75)90030-6.

Akasofu, S.-I. (2013), Where is the magnetic energy for the expansion phase of auroral substorms accumulated?, *J. Geophys. Res. Space Physics*, *118*, 7219–7225, doi:10.1002/2013JA019042.

Akasofu, S.-I., and S. Chapman (1961), The ring current, geomagnetic disturbance, and the Van Allen radiation belts, *J. Geophys. Res.*, *66*(5), 1321–1350, doi:10.1029/JZ066i005p01321.

Anderson, B. J., K. Takahashi, and B. A. Toth (2000), Sensing global Birkeland currents with Iridium®engineering magnetometer data, *Geophys. Res. Lett.*, *27*, 4045–4048.

Birkeland, K. (1908), *The Norwegian Aurora Polaris Expedition 1902–1903*, vol. 1, H. Aschelhoug and Co., Christiania.

Birkeland, K. (1913), *The Norwegian Aurora Polaris Expedition 1902–1903*, vol. 2, H. Aschelhoug and Co., Christiania.

Clauer, C. R., and R. L. McPherron (1974), Mapping the local time-universal time development of magnetospheric substorms using mid-latitude magnetic observations, *J. Geophys. Res.*, *79*(19), 2811–2820, doi:10.1029/JA079i019p02811.

Clausen, L. B. N., J. B. H. Baker, J. M. Ruohoniemi, S. E. Milan, and B. J. Anderson (2012), Dynamics of the region 1 Birkeland current oval derived from the Active Magnetosphere and Planetary Electrodynamics Response Experiment (AMPERE), *J. Geophys. Res.*, *117*, A06233, doi:10.1029/2012JA017666.

Clausen, L. B. N., S. E. Milan, J. B. H. Baker, J. M. Ruohoniemi, K.-H. Glassmeier, J. C. Coxon, and B. J. Anderson (2013a), On the influence of open magnetic flux on substorm intensity: Ground- and space-based observations, *J. Geophys. Res. Space Physics*, *118*, 2958–2969, doi:10.1002/jgra.50308.

Clausen, L. B. N., J. B. H. Baker, J. M. Ruohoniemi, S. E. Milan, J. C. Coxon, S. Wing, S. Ohtani, and B. J. Anderson (2013b), Temporal and spatial dynamics of the regions 1 and 2 Birkeland currents during substorms, *J. Geophys. Res. Space Physics*, *118*, 3007–3016, doi:10.1002/jgra.50288.

Cowley, S. W. H. (2000), Magnetosphere-ionosphere interactions: A tutorial review, in *Magnetospheric Current Systems, Geophys. Monogr. Ser.*, vol. 118, pp. 91–106, AGU, Washington, D. C.

Cowley, S. W. H., and M. Lockwood (1992), Excitation and decay of solar wind-driven flows in the magnetosphere-ionosphere system, *Ann. Geophys.*, *10*, 103–115.

Coxon, J. C., S. E. Milan, L. B. N. Clausen, B. J. Anderson, and H. Korth (2014), The magnitudes of the regions 1 and 2 Birkeland currents observed by AMPERE and their role in solar wind-magnetosphere-ionosphere coupling, *J. Geophys. Res. Space Physics*, doi:10.1002/2014JA020138.

Dungey, J. W. (1961), Interplanetary magnetic field and the auroral zones, *Phys. Rev. Lett.*, *6*, 47–48.

Forsyth, C., et al. (2014), In situ spatiotemporal measurements of the detailed azimuthal substructure of the substorm current wedge, *J. Geophys. Res. Space Physics*, *119*, 927–946, doi:10.1002/2013JA019302.

Freeman, M. P., and S. K. Morley (2009), No evidence for externally triggered substorms based on superposed epoch analysis of IMF Bz, *Geophys. Res. Lett.*, *36*, L21101, doi:10.1029/2009GL040621.

Gjerloev, J. W. (2009), A global ground-based magnetometer initiative, *Eos Trans. AGU*, *90*(27), 230–231, doi:10.1029/2009EO270002.

Gjerloev, J. W. (2012), The SuperMAG data processing technique, *J. Geophys. Res.*, *117*, A09213, doi:10.1029/2012JA017683.

Gjerloev, J. W., R. A. Hoffman, M. M. Friel, L. A. Frank, and J. B. Sigwarth (2004), Substorm behavior of the auroral electrojet indices, *Ann. Geophys.*, *22*(6), 2135–2149, doi:10.5194/angeo-22-2135-2004.

Iijima, T., and T. Nagata (1972), Signatures for substorm development of the growth phase and expansion phase, *Planet. Space Sci.*, *20*(7), 1095–1112, doi:10.1016/0032-0633(72)90219-X.

Iijima, T., and T. A. Potemra (1976a), The amplitude distribution of field-aligned currents at northern high latitudes observed by Triad, *J. Geophys. Res.*, *81*, 2165–2174.

Iijima, T., and T. A. Potemra (1976b), Field-aligned currents in the dayside cusp observed by Triad, *J. Geophys. Res.*, *81*, 5971–5979.

Iijima, T., and T. A. Potemra (1978), Large-scale characteristics of field-aligned currents associated with substorms, *J. Geophys. Res.*, *83*, 599–615.

Kamide, Y., S. Kokubun, L. Bargatze, and L. Frank (1999), The size of the polar cap as an indicator of substorm energy, *Phys. Chem. Earth Part C: Sol. Terr. Planet. Sci.*, *24*(1–3), 119–127, doi:10.1016/S1464-1917(98)00018-X.

King, J. H. (1991), Long-term solar wind variations and associated data sources, *J. Geomagn. Geoelectr.*, *43*(Supplement2), 865–880.

Lockwood, M., and S. W. H. Cowley (1992), Ionospheric convection and the substorm cycle, in *Substorms 1: Proceedings of the First International Conference on Substorms*, vol. 1, pp. 99–109, European Space Agency, Kiruna, Sweden.

McPherron, R. L. (1970), Growth phase of magnetospheric substorms, *J. Geophys. Res.*, *75*(28), 5592–5599, doi:10.1029/JA075i028p05592.

Milan, S. E. (2013), Modeling Birkeland currents in the expanding/contracting polar cap paradigm, *J. Geophys. Res. Space Physics*, *118*, 5532–5542, doi:10.1002/jgra.50393.

Milan, S. E., M. Lester, S. W. H. Cowley, K. Oksavik, M. Brittnacher, R. A. Greenwald, G. Sofko, and J.-P. Villain (2003), Variations in the polar cap area during two substorm cycles, *Ann. Geophys.*, *21*(5), 1121–1140, doi:10.5194/angeo-21-1121-2003.

Milan, S. E., G. Provan, and B. Hubert (2007), Magnetic flux transport in the Dungey cycle: A survey of dayside and nightside reconnection rates, *J. Geophys. Res.*, *112*, A01209, doi:10.1029/2006JA011642.

Milan, S. E., A. Grocott, C. Forsyth, S. M. Imber, P. D. Boakes, and B. Hubert (2009a), A superposed epoch analysis of auroral evolution during substorm growth, onset and recovery: Open magnetic flux control of substorm intensity, *Ann. Geophys.*, *27*(2), 659–668, doi:10.5194/angeo-27-659-2009.

Milan, S. E., J. Hutchinson, P. D. Boakes, and B. Hubert (2009b), Influences on the radius of the auroral oval, *Ann. Geophys.*, *27*, 2913–2924.

Milan, S. E., J. S. Gosling, and B. Hubert (2012), Relationship between interplanetary parameters and the magnetopause reconnection rate quantified from observations of the expanding polar cap, *J. Geophys. Res.*, *117*, A03226, doi:10.1029/2011JA017082.

Murphy, K. R., I. R. Man, I. Jonathan Rae, C. L. Waters, H. U. Frey, A. Kale, H. J. Singer, B. J. Anderson, and H. Korth (2013), The detailed spatial structure of field aligned currents comprising the substorm current wedge, *J. Geophys. Res. Space Physics*, *118*, 7714–7727, doi:10.1002/2013JA018979.

Newell, P. T., and J. W. Gjerloev (2011a), Evaluation of SuperMAG auroral electrojet indices as indicators of substorms and auroral power, *J. Geophys. Res.*, *116*, A12211, doi:10.1029/2011JA016779.

Newell, P. T., and J. W. Gjerloev (2011b), Substorm and magnetosphere characteristic scales inferred from the SuperMAG auroral electrojet indices, *J. Geophys. Res.*, *116*, A12232, doi:10.1029/2011JA016936.

Papitashvili, V. O., N. E. Papitashvili, and J. H. King (2000), Solar cycle effects in planetary geomagnetic activity: Analysis of 36-year long OMNI dataset, *Geophys. Res. Lett.*, *27*(17), 2797–2800, doi:10.1029/2000GL000064.

Rostoker, G., S.-I. Akasofu, J. Foster, R. Greenwald, Y. Kamide, K. Kawasaki, A. Lui, R. McPherron, and C. Russell (1980), Magnetospheric substorms—Definition and signatures, *J. Geophys. Res.*, *85*(A4), 1663–1668, doi:10.1029/JA085iA04p01663.

Sergeev, V. A., A. V. Nikolaev, N. A. Tsyganenko, V. Angelopoulos, A. V. Runov, H. J. Singer, and J. Yang (2014), Testing a two-loop pattern of the substorm current wedge (SCW2L), *J. Geophys. Res. Space Physics*, *119*, 947–963, doi:10.1002/2013JA019629.

Siscoe, G. L., and T. S. Huang (1985), Polar cap inflation and deflation, *J. Geophys. Res.*, *90*(A1), 543–547, doi:10.1029/JA090iA01p00543.